Gap junctions between hippocampal neurons have been shown to exist[17]. CA1 pyramidal cells show calcium- and pH-dependent coupling[10,18,19] and contain connexin-43 messenger RNA[20], indicating that they can form gap junctions. Our results are consistent with the facts that gap-junction coupling is enhanced during intracellular alkalosis[13] (and decreased during acidosis[21]) and that gap-junction coupling is important in synchronous bursts in calcium-free medium[9,22]. Extracellular and intracellular potentials in CA1 pyramidal cells in calcium-free media[10,23] resemble the phenomena observed in our experiments (Fig. 4). Our simulations of pyramidal cells, and previous simulations of interneurons[24], show that as few as 1.6–2.0 gap junctions per cell can lead to synchronous neuronal activity (compare with Fig. 4D). In agreement with our findings, electrotonic coupling can synchronize activity in the developing hippocampus[25] and generate network oscillations in sympathetic preganglionic neurons[26] and the inferior olive[27]. Gap junctions can exist between axons in mammalian retina[28] and ectopic action potentials generated in axons need not invade the soma[29]. Our experiments and simulations indicate that gap junctions may occur between axons in the mammalian forebrain, and may be able to synchronize neuronal activity on a fast time scale. □

Methods

We prepared transverse 400 μm hippocampal slices from Wistar rats of both sexes after anaesthesia, cervical dislocation, brain dissection and cooling to 4 °C in gassed (5% CO_2, 95% O_2) ACSF containing (in mM): NaCl, 135; KCl, 3; NaH_2PO_4, 1.25; $CaCl_2$, 2; $MgCl_2$, 4; glucose, 10; and $NaHCO_3$, 32. Slices were maintained for 1–10 h at room temperature in a gassed, ACSF-filled storage chamber. For recording, we transferred a slice to a chamber mounted on an upright microscope with a ×40 water-immersion objective and differential interference contrast (DIC) optics. The slice was superfused with ACSF at 34–35 °C containing 1 mM Mg^{2+}; in some experiments we used 5 mM KCl to enhance excitability. For field potential measurements we used a microelectrode filled with HEPES-buffered solution (pH 7.4), tip broken to diameter 15–30 μm, a chlorided silver wire reference electrode less than 2 mm from the microelectrode, and differential recordings by a Neurolog 104 amplifier (Digitimer). The signal was filtered at the indicated frequencies with an active filter (Digitimer NL 125). Data were stored and analysed on a PC using SIGNAL software (CED). For whole-cell patch-clamp recordings[30] we used a SEC 5L (npi electronics) in the switched current clamp or bridge mode. Intracellular solution contained (in mM): KCl, 135; $MgCl_2$, 2; $CaCl_2$, 1; HEPES, 10; EGTA, 10; pH, 7.2 (KOH). NBQX (6-nitro-7-sulphamoylbenzo[f]quinoxaline-2,3-dione) and D-AP5(D-2-amino-5-phosphonopentanoic acid) were from RBI; other drugs were from Sigma.

Received 18 March; accepted 21 May 1998.

1. Vanderwolf, C. H. Hippocampal electrical activity and voluntary movement in the rat. *Electroencephalogr. Clin. Neurophysiol.* **26,** 407–418 (1969).
2. Stumpf, C. The fast component in the electrical activity of rabbit's hippocampus. *Electroencephalogr. Clin. Neurophysiol.* **18,** 477–486 (1965).
3. Chrobak, J. J. & Buzsáki, G. High-frequency oscillations in the output network of the hippocampal-entorhinal axis of the freely behaving rat. *J. Neurosci.* **16,** 3056–3066 (1996).
4. Ylinen, A. *et al.* Sharp wave-associated high-frequency oscillation (200 Hz) in the intact hippocampus: network and intracellular mechanisms. *J. Neurosci.* **15,** 30–46 (1995).
5. Buzsáki, G., Horváth, Z., Urioste, R., Hetke, J. & Wise, K. High-frequency network oscillation in the hippocampus. *Science* **256,** 1025–1027 (1992).
6. Cobb, S. R., Buhl, E. H., Halasy, K., Paulsen, O. & Somogyi, P. Synchronization of neuronal activity in hippocampus by individual GABAergic interneurons. *Nature* **378,** 612–615 (1995).
7. Whittington, M. A., Traub, R. D. & Jefferys, J. G. R. Synchronized oscillations in interneuron networks driven by metabotropic glutamate receptor activation. *Nature* **373,** 612–615 (1995).
8. Jefferys, J. G. R. & Haas, H. L. Synchronized bursting of CA1 pyramidal cells in the absence of synaptic transmission. *Nature* **300,** 448–450 (1982).
9. Taylor, C. P. & Dudek, F. E. Synchronous neural afterdischarges in rat hippocampal slices without active chemical synapses. *Science* **218,** 810–812 (1982).
10. Valiante, T. A., Perez-Velazquez, J. L., Jahromi, S. S. & Carlen, P. L. Coupling potentials in A1 neurons during calcium-free-induced field burst activity. *J. Neurosci.* **15,** 6946–6956 (1995).
11. Leslie, J., Nolan, M. F., Logan, S. D. & Spanswick, D. Actions of carbenoxolone on rat sympathetic preganglionic neurones *in vitro*. *J. Physiol. (Lond.)* **506P,** 146 (1998).
12. Thomas, R. C. Experimental displacement of intracellular pH and the mechanism of its subsequent recovery. *J. Physiol. (Lond.)* **354,** 3–22 (1984).
13. Spray, D. C., Harris, A. L. & Bennett, M. V. L. Gap junctional conductance is a simple and sensitive function of intracellular pH. *Science* **211,** 712–715 (1981).
14. Spencer, W. A. & Kandel, E. R. Electrophysiology of hippocampal neurons. IV. Fast prepotentials. *J. Neurophysiol.* **24,** 272–285 (1961).
15. Traub, R. D., Jefferys, J. G. R., Miles, R., Whittington, M. A. & Tóth, K. A branching dendritic model of a rodent CA3 pyramidal neurone. *J. Physiol. (Lond.)* **481,** 79–95 (1994).
16. Jefferys, J. G. R. Influence of electric fields on the excitability of granule cells in guinea-pig hippocampal slices. *J. Physiol. (Lond.)* **319,** 143–152 (1981).
17. Rash, J. *et al.* Grid-mapped freeze-fracture analysis of gap junctions in gray and white matter of adult rat central nervous system, with evidence for a "pan-glial syncytium" that is not coupled to neurons. *J. Comp. Neurol.* **388,** 265–292 (1997).
18. Church, J. & Baimbridge, K. G. Exposure to high-pH medium increases the incidence and extent of dye coupling between rat hippocampal CA1 pyramidal neurons *in vitro*. *J. Neurosci.* **11,** 3289–3295 (1991).
19. MacVicar, B. A. & Dudeck, F. E. Electrotonic coupling between pyramidal cells: a direct demonstration in rat hippocampal slices. *Science* **213,** 782–785 (1981).
20. Simbürger, E., Stang, A., Kremer, M. & Dermietzel, R. Expression of connexin 43 in adult rodent brain. *Histochem. Cell Biol.* **107,** 127–137 (1997).
21. MacVicar, B. A. & Jahnsen, H. Uncoupling of CA3 pyramidal neurons by propionate. *Brain Res.* **330,** 141–145 (1985).
22. Perez-Velazquez, J. L., Valiante, T. A. & Carlen, P. L. Modulation of gap junctional mechanisms during calcium-free induced field burst activity: a possible role for electrotonic coupling in epileptogenesis. *J. Neurosci.* **14,** 4308–4317 (1994).
23. Patrylo, P. R., Kuhn, A. J., Schweitzer, J. S. & Dudeck, F. E. Multiple-unit recordings during slow field-potential shifts in low-$[Ca^{2+}]_0$ solutions in rat hippocampal and cortical slices. *Neuroscience* **74,** 107–118 (1996).
24. Traub, R. D. Model of synchronized population bursts in electrically coupled interneurons containing active dendritic conductances. *J. Comp. Neurosci.* **2,** 283–289 (1995).
25. Strata, F. *et al.* Pacemaker current in dye-coupled hilar interneurons contributes to the generation of giant GABAergic potentials in developing hippocampus. *J. Neurosci.* **17,** 1435–1446 (1997).
26. Logan, S. D., Pickering, A. E., Gibson, I. C., Nolan, M. F. & Spanswick, D. Electrotonic coupling between rat sympathetic preganglionic neurones *in vitro*. *J. Physiol. (Lond.)* **495,** 491–502 (1996).
27. Llinás, R., Baker, R. & Sotelo, C. Electrotonic coupling between neurons in cat inferior olive. *J. Neurophysiol.* **37,** 560–571 (1974).
28. Vaney, D. I. The coupling pattern of axon-bearing horizontal cells in the mammalian retina. *Proc. R. Soc. Lond. B* **252,** 93–101 (1993).
29. Pinault, D. Backpropagation of action potentials generated at ectopic axonal loci: hypothesis that axon terminals integrate local environmental signals. *Brain Res. Brain Res. Rev.* **21,** 42–92 (1995).
30. Hamill, O. P., Marty, A., Neher, E., Sakmann, B. & Sigworth, F. J. Improved patch-clamp techniques for high-resolution recording from cells and cell-free membrane patches. *Pflügers Arch.* **391,** 85–81 (1981).

Acknowledgements. This work was supported by a Training grant from the European Commission (to A.D.) and by the Wellcome Trust. R.D.T. is a Wellcome Principal Research Fellow. We thank U. Heinemann, H.-J. Gabriel, S. Gabriel and U. Endermann for discussions.

Correspondence and requests for materials should be addressed to A.D. (draguhn@rz.charite.hu-berlin.de).

Visualizing secretion and synaptic transmission with pH-sensitive green fluorescent proteins

Gero Miesenböck, Dino A. De Angelis & James E. Rothman

Cellular Biochemistry and Biophysics Program, Memorial Sloan-Kettering Cancer Center, 1275 York Avenue, New York, New York 10021, USA

In neural systems, information is often carried by ensembles of cells rather than by individual units. Optical indicators[1] provide a powerful means to reveal such distributed activity, particularly when protein-based and encodable in DNA[2–4]: encodable probes can be introduced into cells, tissues, or transgenic organisms by genetic manipulation, selectively expressed in anatomically or functionally defined groups of cells, and, ideally, recorded *in situ*, without a requirement for exogenous cofactors. Here we describe sensors for secretion and neurotransmission that fulfil these criteria. We have developed pH-sensitive mutants of green fluorescent protein ('pHluorins') by structure-directed combinatorial mutagenesis, with the aim of exploiting the acidic pH inside secretory vesicles[5,6] to monitor vesicle exocytosis and recycling. When linked to a vesicle membrane protein, pHluorins were sorted to secretory and synaptic vesicles and reported transmission at individual synaptic boutons, as well as secretion and fusion pore 'flicker' of single secretory granules.

Wild-type green fluorescent protein (GFP) has a bimodal excitation spectrum[7,8] with peaks at 395 and 475 nm (Fig. 1a). Underlying the two maxima are protonated and deprotonated states of Tyr 66, which forms part of the chromophore[9–13]. Although critical residues exchange protons with the environment[10], the excitation spectrum of GFP is essentially unaltered between pH 5.5 and 10 (ref. 7 and

Fig. 1a). This implies that protonation–deprotonation reactions are constrained; a given GFP is trapped in either of two alternative conformations: in one the chromophore is protonated and can be excited at 395 nm, and in the other it is deprotonated and can be excited at 475 nm.

We surmised that converting GFP to a pH sensor would require amino-acid substitutions that facilitate switching between conformers, or that couple changes in bulk pH to changes in the electrostatic environment of the chromophore. To obtain such substitutions, we focused on seven key positions (Gln 94, Arg 96, His 148, Ile 167, Thr 203, Ser 205 and Glu 222) known from X-ray crystallography[11–13] to be part of the proton-relay network of Tyr 66 or to alter the excitation spectrum when mutated[9,11,14,15].

Because histidine has the desired pK_a for a sensor for exocytosis, we introduced histidines at positions flanking key residues. One such mutant, S202H, showed a 16% reduction in 395-nm excitation with a 26% increase in 475-nm excitation, induced by a pH shift from 7.4 to 6.0. S202H provided the starting point for a combinatorial enhancement of pH sensitivity. Complementary DNAs of S202H (or of intermediates obtained in later rounds) were amplified by using primers in a polymerase chain reaction (PCR) that simultaneously altered between one and five codons and encoded between 20 and 8,000 different polypeptide sequences. The GFP libraries were expressed in *Escherichia coli* and a total of ~19,000 fluorescent colonies screened for pH sensitivity (see Methods). Several rounds of mutagenesis generated two classes of pH-sensitive fluorescent proteins ('pHluorins'), which we term 'ratiometric' and 'ecliptic'.

Ratiometric pHluorin contains the original mutation S202H plus E132D, S147E, N149L, N164I, K166Q, I167V, R168H and L220F.

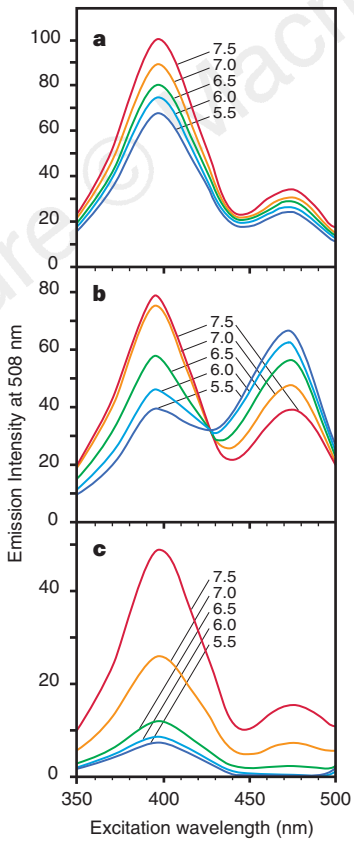

Figure 1 Fluorescence excitation spectra. **a**, Wild-type GFP; **b**, ratiometric pHluorin; and **c**, ecliptic pHluorin. Samples contained 27.5 μM chromophore in 50 mM sodium cacodylate plus 50 mM sodium acetate, adjusted to the indicated pH values, and 100 mM NaCl, 1 mM $CaCl_2$, 1 mM $MgCl_2$. The ordinate scales reflect normalized differences in emitted fluorescence intensity.

The protein displays a reversible excitation ratio change between pH 7.5 and 5.5 (Fig. 1b), with a response time of <20 ms (not shown). Ecliptic pHluorin, by contrast, gradually loses fluorescence as pH is lowered, until at pH values of <6.0, the excitation peak at 475 nm vanishes (Fig. 1c). In an environment of pH <6.0, the protein is therefore invisible (eclipsed) under 475-nm excitation but can still be weakly seen at 395 nm. These changes are reversible within <20 ms after returning to neutral pH (not shown). Ecliptic pHluorin no longer contains S202H but carries the substitutions S147D, N149Q, T161I, S202F, Q204T and A206T. For both pHluorins, neither the minimal set of mutations nor the mechanism by which they confer pH sensitivity has been delineated. However, association of monomers into dimers[8,12] or dissociation of existing dimers do not seem to be involved (results not shown).

For initial imaging experiments, ratiometric pHluorins were glycosylphosphatidylinositol(GPI)-anchored[16] at the cell surface (Fig. 2b), inserted into the lumenal domain of TGN38 (ref. 17), a membrane protein of the *trans*-Golgi network (TGN) (Fig. 2c), or attached to the lumenally exposed carboxy terminus of cellubrevin[18], an endosomal membrane protein (Fig. 2d). Correct targeting of these constructs was confirmed by co-localization with standard markers (results not shown). The labelled subcellular compartments of transfected HeLa cells were readily seen by wide-field fluorescence microscopy and characterized by distinct 410/470-nm excitation ratios, $R_{410/470}$ (Fig. 2). The ratios remained stable within ±3% during 2 min of continuous image acquisition at 1 Hz, indicating lack of photoisomerization[13].

Table 1 Ratiometric pHluorin as an indicator of synaptic transmission

Nerve terminal	$R_{410/470}$	r.m.s. noise
Resting (n = 18)	0.418 ± 0.021	0.016 ± 0.003
Depolarized		
+Ca^{2+} (n = 18)	0.479 ± 0.020*	0.023 ± 0.005*
–Ca^{2+} (n = 18)	0.416 ± 0.017	0.016 ± 0.005
+BoNT B (n = 18)	0.421 ± 0.021	0.017 ± 0.003

$R_{410/470}$ and r.m.s. noise (± s.d.) in recordings from individual synaptic boutons, obtained at 1 Hz. Evaluation windows extended over 10 s, starting at 3 s after application of a depolarizing stimulus. Significant differences ($P < 0.01$) with respect to resting conditions are indicated by asterisks.

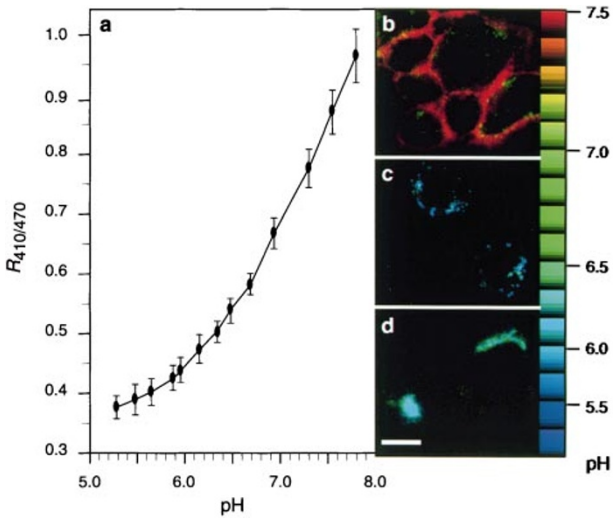

Figure 2 pH measurements with ratiometric pHluorin in HeLa cells. **a**, Calibration curve of $R_{410/470}$ (mean ± s.d.). Cells expressing GPI-anchored ratiometric pHluorin at their surface (n = 28) were imaged in buffers adjusted to pH values between 5.28 and 7.8. **b–d**, Ratiometric pH measurements in subcellular compartments, colour-encoded according to the look-up table on the right. Targeting modules used: **b**, GPI anchor for delivery to the cell surface (at pH 7.40); **c**, cellubrevin for sorting to endosomes; **d**, TGN38 for localization to the *trans*-Golgi network. Scale bar, 10 μm.

To convert excitation ratios to pH values, cells expressing GPI-anchored pHluorin at their surface were imaged in buffers of defined pH. Based on this standard curve (Fig. 2a), we determined pH values (mean ± s.d.) of 5.51 ± 0.66 for endosomes ($n = 61$) and 6.21 ± 0.39 for the TGN ($n = 28$), consistent with previous estimates[5].

Fusion of an acidified vesicle[5,6] with the plasma membrane will establish continuity of its interior with the extracellular fluid and cause an instantaneous rise of pH to ~7.4. A pHluorin, attached to the inner surface of the vesicle membrane, will reflect this pH change in its excitation spectrum. Figure 3a shows a field of hippocampal neurons[2] forming abundant synapses revealed by immunostaining for synaptotagmin-I (ref. 6). Some of these synapses were made by neurons infected with a herpes simplex virus (HSV) vector[2,19,20] expressing synapto-pHluorin, a fusion protein of VAMP-2/synaptobrevin[6] and the ratiometric pHluorin, joined to VAMP at its lumenally exposed C terminus (Fig. 3b).

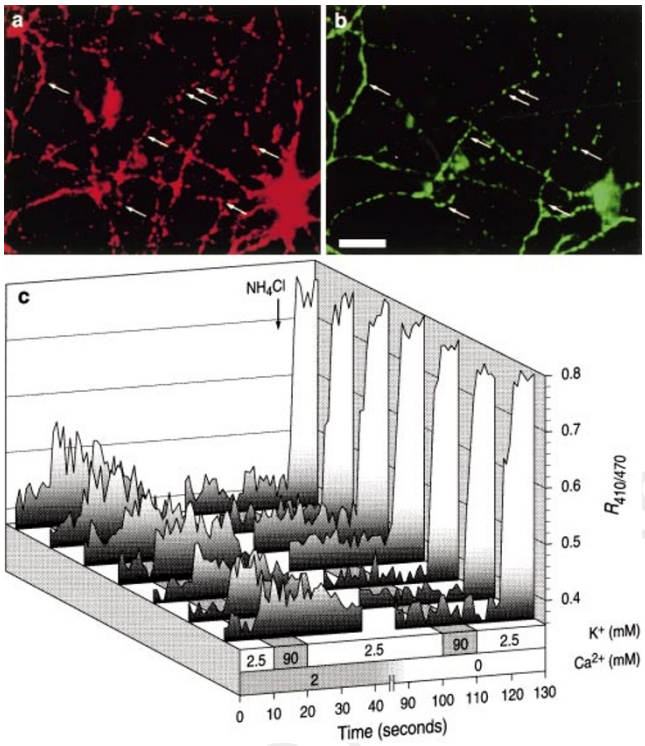

Figure 3 Neurotransmission visualized with ratiometric pHluorin. **a**, Hippocampal neurons immunostained with a monoclonal antibody against synaptotagmin-I. **b**, Synapses expressing synapto-pHluorin, formed by HSV-infected neurons whose somata lie outside the field of view. Arrows mark some points of registration between **a** and **b**. Scale bar, 20 μm. **c**, Recordings of synaptic activity from seven boutons, sampled at 1 Hz. Neurons were stepped through two depolarization cycles (by raising extracellular [K^+] to 90 mM), the first in 2 mM extracellular Ca^{2+} and the second in the absence of Ca^{2+} and the presence of 2.5 mM EGTA.

Under resting conditions, the synapto-pHluorin reported an intravesicular pH (mean ± s.d.) of 5.67 ± 0.71 ($n = 84$). Depolarization with 90 mM KCl elicited a prompt increase in $R_{410/470}$ which could be recorded from many boutons in parallel (Fig. 3c). The response depended on external Ca^{2+} (Fig. 3c and Table 1) and was abolished by a 24-hour preincubation with 10 nM botulinum neurotoxin B (BoNT; ref. 6) (Table 1). $R_{410/470}$ peaked at 8–20% of the signal that would have resulted from simultaneous fusion of all of the vesicles in the bouton; the latter was estimated by neutralizing the pH in all vesicles with 50 mM NH_4Cl (Fig. 3c). The increase in $R_{410/470}$ most probably corresponds to the 'readily releasable' pool[6,21] of one to two dozen[21] of the 100–200 synaptic vesicles at an active zone[6].

Following repolarization, $R_{410/470}$ gradually declined (Fig. 3c). Vesicle membrane protein is re-internalized by endocytosis[6] to regenerate synaptic vesicles, and synapto-pHluorin is expected to return to its spectral baseline as the vesicle acidifies. The $R_{410/470}$ value, whether it pertains to a single synapse or to a population of many synapses in a region, therefore provides a running average of activity during the previous several seconds.

Ecliptic pHluorins, because they are non-fluorescent at pH <6 under 470-nm excitation (Fig. 1c), eliminate background due to resting vesicles and are thus potentially suited for detecting single vesicle fusion events. To test this in a favourable case, ecliptic synapto-pHluorin (a fusion protein of VAMP and the ecliptic pHluorin) was expressed in the mast cell line RBL-2H3 (ref. 22). The protein localized to scattered fluorescent puncta, which under resting conditions were seen only with 410- but not 470-nm excitation (Fig. 4a, frame 1); the pH in these secretory granules, measured with the ratiometric pHluorin, averaged (mean ± s.d.) 5.20 ± 0.55 ($n = 29$).

After initiating a secretory response[22], granule content was released into the medium (Fig. 4b), and changes in fluorescence excited at 470 nm occurred in locations harbouring granules (Fig. 4a, frames 1–7). Individual spots of variable integrated intensity (Fig. 4c) appeared suddenly at various times after the stimulus to secrete (Fig. 4a, frames 2–7). The appearance of fluorescence followed the

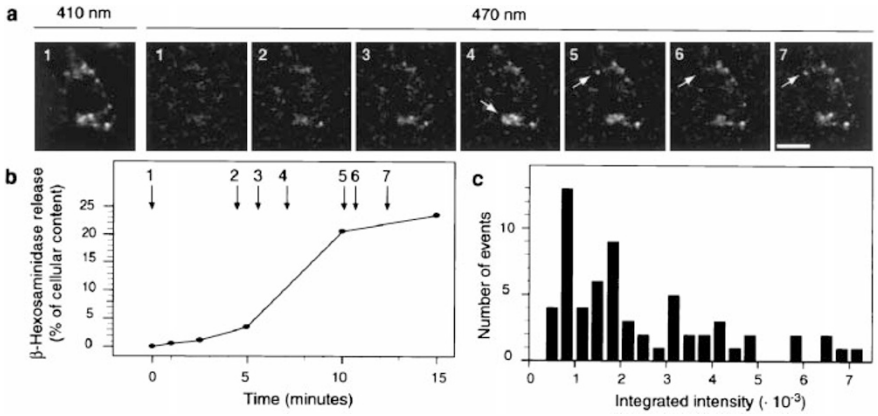

Figure 4 Secretion visualized with ecliptic pHluorin. **a**, RBL-2H3 cells under resting conditions (frame 1) and after triggering exocytosis (frames 2–7). Arrows mark a cluster from which individual spots are disappearing (frame 4), and a 'flickering' spot (frames 5–7). Images were contrast-enhanced and low-pass-filtered with a 3 × 3 binomial kernel. Scale bar, 10 μm. **b**, Release of β-hexosaminidase, a marker enzyme of RBL cell granules[22]. Times at which frames in **a** were acquired are indicated by arrows. **c**, Size distribution of secretory events. Integrated intensity is the product of pixel area and average fluorescence intensity.

appearance of granule content in the medium (Fig. 4b), as would be expected if each event were due to fusion of a single granule[23], or of multiple granules undergoing compound exocytosis[23,24].

Occasionally, fluorescent spots disappeared, indicating granule retrieval and re-acidification (follow the cluster marked by the arrow in frame 4 through frames 5 and 6). Within the time frame of our experiments (Fig. 4b), these 'off' events[23] were less frequent than the 'on' events of exocytosis, consistent with slow resolution of the often tortuous membrane topology created at exocytosis sites[24]. Rarely, a granule appeared, disappeared, and reappeared in what seemed to be the same location (arrows in frames 5–7). This could correspond to the phenomenon of 'flicker'[23], in which transient opening and closing of a fusion pore would cause the vesicle's internal pH (and the pHluorin's emission intensity) to fluctuate.

The pHluorin technique may be extended to preparations other than cultured cells, trafficking processes other than exocytosis, and read-out formats other than fluorescence microscopy. For examples, ecliptic synapto-pHluorins imaged by two-photon or confocal microscopy could sensitively report transmission in neural tissues of transgenic animals, in a transmitter- or cell type-specific manner. Generally, pHluorins should be capable of monitoring pathways that connect compartments of differing pH, from receptor-mediated endocytosis[5] to internalization of activated signalling receptors[25,26] or insulin-dependent translocation of glucose transporters from internal stores to the cell surface[27]. Many of these processes involve potential drug targets, and pHluorins could be adapted to cell- or tissue-based assays for high-throughput screening of compound libraries. □

Methods

Mutagenesis. Wild-type *Aequorea victoria gfp* cDNA (pGFP-1; Clontech) was subjected to PCR mutagenesis. Directed codon changes were introduced with *Pwo* polymerase; combinatorial steps (codons 94–97, 146–149, 164–168, 202–205, 221–225) used primer libraries of 32- to 32,768-fold nucleotide degeneracy and *Taq* polymerase. PCR products were ligated to pGEMEX-2 (Promega), transformed into *E. coli*, and visibly fluorescent colonies expanded for analysis. Clones were grown, lysed (50 mM Tris, pH 8.0, 2 mM EDTA, 0.2 mg ml^{-1} lysozyme, 200 U ml^{-1} DNase I), and analysed in 96-well plates. Three fluorescence readings at 510 nm were obtained in a Labsystems Fluoroskan II plate reader equipped with 400- and 460-nm excitation filters: the first at pH 8.0, the second after addition of acid to reduce the pH to 6.0, and the third after addition of base to revert the pH to 7.4. The plasmid encoding the mutant with the largest reversible change served as the PCR template in the next round.

cDNAs encoding ratiometric and ecliptic pHluorins—both of which also carry two amino-acid changes (V163A, S175G) that are known to improve folding[28] at 37 °C—were sequenced and expressed in pGEX-2T (Pharmacia). Fluorescence spectra were recorded on material obtained after thrombin cleavage of the respective glutathione-*S*-transferase (GST) fusion protein, in a Perkin-Elmer LS-50B spectrofluorimeter with 8-nm bandwidths for excitation and emission. Chromophore concentrations are based on the 447-nm absorbance at pH 11.8 of denatured GFP or pHluorin and an extinction coefficient[7] of 44,100 M^{-1} cm^{-1}. Response times to pH jumps were estimated with the help of an SFA-20 rapid kinetics accessory (Hi-Tech Scientific).

Cells. GFP modules were linked to targeting modules via two -Ser-Gly-Gly- repeats and one -Thr-Gly-Gly- repeat. The insertion sites were placed between signals for translocation into the endoplasmic reticulum and GPI-anchor addition (derived from preprolactin and decay accelerating factor[16], respectively), at the mature N terminus of TGN38 (ref. 17) and at the C termini of VAMP[6] and cellubrevin[18].

The vector pCI (Promega) was used to drive expression in HeLa and RBL-2H3 cells. Cell-surface IgE receptors of RBL-2H3 cells were loaded with 10 ng ml^{-1} anti-DNP IgE (Sigma) and secretory responses triggered with 1 μg ml^{-1} anti-IgE antibodies (PharMingen). β-Hexosaminidase was assayed as described[22].

Hippocampal neurons were infected with THZ.3 ($\alpha4^-$, $\alpha22^-$, $\alpha27^-$, U_L41^-) HSV virions[19] carrying amplicon plasmids based on the pα4′a′ backbone[20]. Neural cultures were prepared as described[2], except that hippocampi were collected from E19 rats, horse serum was used, and 10 μM cytosine arabinoside was added from day 3 after plating. Experiments were done after 17–29 days *in vitro*.

Microscopy. Two days after transfection or viral infection, cells in imaging buffer (25 mM Na-HEPES, pH 7.4, 119 mM NaCl, 2.5 mM KCl, 2 mM $CaCl_2$, 2 mM $MgCl_2$, 30 mM glucose) were analysed at 37 °C on a Zeiss Axiovert microscope equipped with a ×40, 1.3 NA Plan-Neofluar objective and ×1.6 and ×2.5 Optovar inserts. Experiments were controlled through MetaFluor 3.0 (Universal Imaging), with off-line background subtraction and image analysis, using MetaMorph 3.0 (Universal Imaging) and Mathematica 3.0 (Wolfram Research). A Polychrome II monochromator (Till Photonics) delivered 12-nm excitation bands centred at 410 and 470 nm and found optimal for imaging. Emitted light passed through a dichromatic mirror (500DCXR) and a bandpass filter (HQ535/50, both from Chroma Technologies) and was collected on an intensified PentaMAX-512EFT frame-transfer camera (Princeton Instruments).

Received 30 January; accepted 1 May 1998.

1. Tsien, R. Y. Fluorescent probes of cell signaling. *Annu. Rev. Neurosci.* **12,** 227–253 (1989).
2. Miesenböck, G. & Rothman, J. E. Patterns of synaptic activity in neural networks recorded by light emission from synaptolucins. *Proc. Natl Acad. Sci. USA* **94,** 3402–3407 (1997).
3. Miyawaki, A. *et al.* Fluorescent indicators for Ca^{2+} based on green fluorescent proteins and calmodulin. *Nature* **388,** 882–887 (1997).
4. Romoser, V. A., Hinkle, P. M. & Persechini, A. Detection in living cells of Ca^{2+}-dependent changes in the fluorescence emission of an indicator composed of two green fluorescent protein variants linked by a calmodulin-binding sequence. *J. Biol. Chem.* **272,** 13270–13274 (1997).
5. Anderson, R. G. & Orci, L. A view of acidic intracellular compartments. *J. Cell Biol.* **106,** 539–543 (1988).
6. Südhof, T. C. The synaptic vesicle cycle: a cascade of protein–protein interactions. *Nature* **375,** 645–653 (1995).
7. Ward, W. W. in *Bioluminescence and Chemiluminescence* (eds DeLuca, M. A. & McElroy, W. D.) 235–242 (Academic, New York, 1981).
8. Ward, W. W., Prentice, H. J., Roth, A. F., Cody, C. W. & Reeves, S. C. Spectral perturbations of the *Aequorea* green-fluorescent protein. *Photochem. Photobiol.* **35,** 803–808 (1982).
9. Heim, R., Prasher, D. C. & Tsien, R. Y. Wavelength mutations and posttranslational autoxidation of green fluorescent protein. *Proc. Natl Acad. Sci. USA* **91,** 12501–12504 (1994).
10. Chattoraj, M., King, B. A., Bublitz, G. U. & Boxer, S. G. Ultra-fast excited state dynamics in green fluorescent protein: Multiple states and proton transfer. *Proc. Natl Acad. Sci. USA* **93,** 8362–8367 (1996).
11. Ormö, M. *et al.* Crystal structure of the *Aequorea victoria* green fluorescent protein. *Science* **273,** 1392–1395 (1996).
12. Yang, F., Moss, L. G. & Phillips, G. N. Jr The molecular structure of green fluorescent protein. *Nature Biotechnol.* **14,** 1246–1251 (1996).
13. Brejc, K. *et al.* Structural basis for dual excitation and photoisomerization of the *Aequorea victoria* green fluorescent protein. *Proc. Natl Acad. Sci. USA* **94,** 2306–2311 (1997).
14. Ehrig, T., O'Kane, D. J. & Prendergast, F. G. Green-fluorescent protein mutants with altered fluorescence excitation spectra. *FEBS Lett.* **367,** 163–166 (1995).
15. Heim, R. & Tsien, R. Y. Engineering green fluorescent protein for improved brightness, longer wavelengths and fluorescence resonance energy transfer. *Curr. Biol.* **6,** 178–182 (1996).
16. Caras, I. W., Weddell, G. N., Davitz, M. A., Nussenzweig, V. & Martin, D. W. Jr Signal for attachment of a phospholipid membrane anchor in decay accelerating factor. *Science* **238,** 1280–1283 (1987).
17. Luzio, J. P. *et al.* Identification, sequencing and expression of an integral membrane protein of the trans-Golgi network (TGN38). *Biochem. J.* **270,** 97–102 (1990).
18. McMahon, H. T. *et al.* Cellubrevin is a ubiquitous tetanus-toxin substrate homologous to a putative synaptic vesicle fusion protein. *Nature* **364,** 346–349 (1993).
19. Marconi, P. *et al.* Replication-defective herpes simplex virus vectors for gene transfer *in vivo*. *Proc. Natl Acad. Sci. USA* **93,** 11319–11320 (1996).
20. Lawrence, M. S., Ho, D. Y., Dash, R. & Sapolsky, R. M. Herpes simplex virus vectors overexpressing the glucose transporter gene protect against seizure-induced neuron loss. *Proc. Natl Acad. Sci. USA* **92,** 7247–7251 (1995).
21. Stevens, C. F. & Tsujimoto, T. Estimates for the pool size of releasable quanta at a single central synapse and for the time required to refill the pool. *Proc. Natl Acad. Sci. USA* **92,** 846–849 (1995).
22. Roa, M., Paumet, F., Le Mao, J., David, B. & Blank, U. Involvement of the *ras*-like GTPase rab3d in RBL-2H3 mast cell exocytosis following stimulation via high-affinity IgE receptors (FcεRI). *J. Immunol.* **159,** 2815–2823 (1997).
23. Fernandez, J. M., Neher, E. & Gomperts, B. D. Capacitance measurements reveal stepwise fusion events in degranulating mast cells. *Nature* **312,** 453–455 (1984).
24. Chandler, D. E. & Heuser, J. E. Arrest of membrane fusion events in mast cells by quick-freezing. *J. Cell Biol.* **86,** 666–674 (1980).
25. Ullrich, A. & Schlessinger, J. Signal transduction by receptors with tyrosine kinase activity. *Cell* **61,** 203–212 (1990).
26. Yu, S. S., Lefkowitz, R. J. & Hausdorff, W. P. β-Adrenergic receptor sequestration: A potential mechanism of receptor resensitization. *J. Biol. Chem.* **268,** 337–341 (1993).
27. James, D. E. & Piper, R. C. Insulin resistance, diabetes, and the insulin-regulated trafficking of GLUT-4. *J. Cell Biol.* **126,** 1123–1126 (1994).
28. Siemering, K. R., Golbik, R., Sever, R. & Haseloff, J. Mutations that suppress the thermosensitivity of green fluorescent protein. *Curr. Biol.* **6,** 1653–1663 (1996).

Acknowledgements. We thank R. Miller for technical assistance, D. Krisky and J. Glorioso for HSV strain THZ.3 and 7B cells, G. Schiavo for BoNT, the Fonds de la Recherche en Santé du Québec for a postdoctoral fellowship (to D.A.D.), and Q. Al-Awqati for discussion. This research was supported by the G. Harold and Leila Y. Mathers Charitable Foundation.

Correspondence and requests for materials should be addressed to J.E.R. The GenBank accession numbers for ratiometric and ecliptic pHluorin are AF058694 and AF058695, respectively.